

X-RAY MODELING OF VERY YOUNG EARLY TYPE STARS IN THE ORION TRAPEZIUM: SIGNATURES OF MAGNETICALLY CONFINED PLASMAS AND EVOLUTIONARY IMPLICATIONS

N.S. SCHULZ,¹ C.CANIZARES,¹ D.HUENEMOERDER,¹ K. TIBBETS¹

accepted for publication in The Astrophysical Main Journal

ABSTRACT

The Orion Trapezium is one of the youngest and closest star forming regions within our Galaxy. With a dynamic age of $\sim 3 \times 10^5$ yr it harbors a number of very young hot stars, which likely are on the zero-age main sequence (ZAMS). We analyzed high resolution X-ray spectra in the wavelength range of 1.5 – 25 Å of three of its X-ray brightest members (Θ^1 Ori A, C and E) obtained with the High Energy Transmission Grating Spectrometer (HETGS) on-board the Chandra X-ray Observatory. We measured X-ray emission lines, calculated differential emission measure distributions (DEMs), and fitted broad-band models to the spectra. The spectra from all three stars are very rich in emission lines, specifically from highly ionized Fe which includes emission from Fe XVII to Fe XXV ions. A complete line list is included. This is a mere effect of high temperatures rather than an overabundance of Fe, which in fact turns out to be underabundant in all three Trapezium members. Similarly there is a significant underabundance in Ne and O as well, whereas Mg, Si, S, Ar, and Ca appear close to solar. The DEM derived from over 80 emission lines in the spectrum of Θ^1 Ori C indicates three peaks located at 7.9 MK, 25 MK, and 66 MK. The emission measure varies over the 15.4 day wind period of the star. For the two phases observed, the low temperature emission remains stable, while the high temperature emission shows significant differences. The line widths seem to show a similar bifurcation, where we resolve some of the soft X-ray lines with velocities up to 850 km s⁻¹ (all widths are stated as FWHM), whereas the bulk of the lines remain unresolved with a confidence limit of 110 km s⁻¹. The broad band spectra of the other two stars can be fitted with several collisionally ionized plasma model components within a temperature range of 4.3 – 46.8 MK for Θ^1 Ori E and 4.8 – 42.7 MK for Θ^1 Ori A. The high temperature emissivity contributes over 70% to the total X-ray flux. None of the lines are resolved for Θ^1 Ori A and E with a confidence limit of 160 km s⁻¹. The influence of the strong UV radiation field on the forbidden line in the He-like triplets allows us to set an upper limit on distance of the line emitting region from the photosphere. The bulk of the X-ray emission cannot be produced by shock instabilities in a radiation driven wind and are likely the result of magnetic confinement in all three stars. Although confinement models cannot explain all the results, the resemblance of the unresolved lines and the of the DEM with recent observations of active coronae in II Peg and AR Lac during flares is quite obvious. Thus we speculate that the X-ray production mechanism in these stars is similar with the difference that the Orion stars maybe in a state of almost continuous flaring driven by the wind. We clearly rule out major effects due to X-rays from a possible companion. The fact that all three stars appear to be magnetic and are near zero age on the main sequence also raises the issue whether the Orion stars are simply different or whether young massive stars enter the main sequence carrying significant magnetic fields. The ratio $\log L_x/L_{bol}$ using the ‘wind’ component of the spectrum is -7 for the Trapezium consistent with the expectation from O-stars. This suggests that massive ZAMS stars generate their X-ray luminosities like normal O stars and magnetic confinement provides an additional source of X-rays.

Subject headings: stars: formation — stars: early-type — X-rays: stars — techniques: spectroscopic — open clusters and associations: individual (Orion Trapezium) — plasmas

1. INTRODUCTION

Since the discovery of X-ray emission from massive early type stars more than two decades ago (Seward et al. 1979, Harnden et al. 1979) it is an ongoing quest to explain its origins and to develop physical models that consistently predict its characteristics. Although to date no definitive models for the production of X-rays in stellar winds exist, it is widely established that X-rays are produced by shocks forming from instabilities within a radiatively driven wind (Lucy & White 1980). This phenomenological model has been revised and expanded throughout the years. Lucy (1982) showed that these shocks can exist well out into the terminal flow overcoming the attenuation problem of the previous model. Owocki, Castor, and Rybicki (1988) extended the model in that they showed that re-

verse shocks are much stronger than forward shocks in an high velocity gas at low densities, deduced from P Cygni absorption in UV resonance line profiles (Puls et al. 1993, Hillier et al. 1993). These models were able to successfully explain the mass loss from a hot luminous star in the UV domain as well as the soft X-ray spectral temperatures, but to date cannot correctly predict observed X-ray fluxes. For example, Feldmeier, Puls & Pauldrach (1997) see the possibility of mutual collisions of dense gas shells in the outer wind to produce stronger shocks. Claims that the X-ray emission could originate from coronal gas near the stellar photosphere were soon considered unlikely due to the lack of soft X-ray absorption edges (Cassinelli & Swank 1983) as well as the absence of coronal emission lines in optical spectra (Nordsieck, Cassinelli, & Anderson 1981).

That all O and early type B stars are strong stellar X-ray

¹Center for Space Research, Massachusetts Institute of Technology, Cambridge MA 02139, USA

emitters is now a well established fact thanks to relentless observations with *Einstein* and *ROSAT* (Pallavicini et al. 1981, Chlebowski et al. 1989, Berghöfer et al. 1994, Cassinelli et al. 1994). Typical X-ray luminosities are of the order of 10^{32} erg s⁻¹ for O-stars and $10^{30.5}$ - $10^{31.5}$ erg s⁻¹ for B-stars (Berghöfer, Schmitt, and Cassinelli 1996), while many low-mass (late type) PMS stars radiate at orders of magnitude lower luminosity and only the peak of their luminosity function reaches 10^{31} erg s⁻¹ (Feigelson and Montmerle 1999). Due to the lack of spectral resolving power, however, many results from *Einstein* and *ROSAT* were based on statistical properties of a large sample of Stars (Chlebowski et al. 1989, Berghöfer, Schmitt, and Cassinelli 1996). Among these results were that the X-ray luminosity in early type stars typically scales with the bolometric luminosity with $\log(L_x/L_{bol}) = -7$ and with a few exceptions as high as -5.

In the first very detailed spectral analysis using the ROSAT PSPC, Hillier et al. (1993) fitted spectra of ζ Pup with NLTE models under the assumptions that the X-rays arise from shocks distributed throughout the wind and that recombination occurs in the outer regions of the stellar wind. The best fits predicted two temperatures of $\log T(\text{K}) \sim 6.2$ to 6.7 with shock velocities around 500 km s^{-1} . Based on this approach, Feldmeier et al. (1997) added the assumption that the X-rays originate from adiabatically expanding cooling zones behind shock fronts and described the spectra with post shock temperature and a volume filling factor. These results were also compared to results from Cohen et al. (1996), who used *ROSAT* and *EUVE* data to constrain high-temperature emission models in the analysis of the B-giant, $p3. \epsilon$ CMA. A continuous temperature distribution was inferred over single or even two temperature models. The result of that comparison remained inconclusive, since both views appeared indistinguishable in the spectra. Despite the success of the wind shock models, several unanswered issues remain from the *Einstein*, *ROSAT*, and *ASCA* era, which seem to be quite in contrast to this model (see also below). One issue concerns the unusually hard X-ray spectra of the B0.2 V star τ Sco observed with *ASCA* (Cohen, Cassinelli, & Waldron 1997), of λ Ori (Corcoran et al. 1994), and of *ROSAT* spectra of stars later than of B2 type (Cohen, Cassinelli, & MacFarlane 1997).

With the availability of high resolution spectra from *Chandra* and *XMM-Newton* the spectral situation became much more complex and confusing. The first published high resolution X-ray spectrum of the Orion Trapezium star Θ^1 Ori C showed extreme temperatures and symmetric lines (Schulz et al. 2000 – paper I). These properties are not expected from shocked material near or beyond regions where the wind reached its terminal velocity. Based on a soft X-ray spectrum and symmetric emission lines from ζ Ori, Waldron and Cassinelli (2001) argued that the emitting plasma originates likely near the photosphere. Highly resolved spectra from ζ Pup with *XMM-Newton* (Kahn et al. 2001) and *Chandra* (Cassinelli et al. 2001) finally showed some expected emission characteristics, i.e. moderate temperatures of 5 to 10 MK, blue shifted and asymmetric lines. Such X-ray line profiles (Ignace 2001, Owocki and Cohen 2001) are significant characteristics of attenuated plasma moving X-ray emitting plasma. Schulz et al. (2001a) and Schulz et al. (2002) report on similar evidence from line profiles in HD 206267 and ι Ori, respectively.

The fact that the Orion Trapezium star Θ^1 Ori C shows such rather strange X-ray characteristics may not come as too much of a surprise, since this star was already known to be of rather peculiar nature (Stahl et al. 1995, Gagne et al. 1997). Babel and Montmerle (1997) proposed an aligned magnetic rotator model. The Orion Trapezium region has always been quite difficult to observe prior to *Chandra* simply for the fact that its constituent members could never be spatially resolved. The *ROSAT* HRI (Gagne et al. 1995) provided better spatial resolution, but no spectral information. Yamauchi and Koyama (1993) observed hard X-rays from the Orion Nebula region with *GINGA* that did not rule out the possibility of 2-3 keV X-rays from Θ^1 Ori C, but focused more on possible hard extended emission within the Nebula. This issue was further studied with *ASCA* (Yamauchi et al. 1996). Highly resolved images and spectra with *Chandra* could clearly resolve this issue. Schulz et al. 2001 fully resolved the Orion Trapezium in the X-ray band between 0.1 and 10 keV and found no diffuse emission between the Trapezium stars. Furthermore four out of five of the brightest Trapezium stars showed hard X-ray spectra, with Θ^1 Ori C being the hottest star showing temperatures of up to 6×10^7 K (paper I).

In this paper we further investigate these issues through detailed modeling of High Energy Transmission Grating Spectrometer (HEGTS) spectra from the three X-ray brightest Trapezium stars Θ^1 Ori A, C, and E (Schulz et al. 2001). These stars are excellent candidates for such a common study since they are presumably very young; the median age of the Orion Trapezium Cluster is 0.3 Myr (Hillenbrand 1997), they were born at the same time and should have had a quite similar initial chemical conditions. Their spectral types range from O6.5V to B3.

2. CHANDRA OBSERVATIONS

We accumulate our spectra from two observations in the early phases of the *Chandra* mission. The first observation was performed on October 31st UT 05:47:21 1999 (OBSID 3) and lasted 50 ks. The second observation was obtained about three weeks later on November 24th UT 05:37:54 1999 (OBSID 4) and lasted 33 ks. For more details of the observations and some of the analysis threads we refer to paper I and Schulz et al. (2001).

2.1. Data Analysis

We re-processed the data using the most recently available calibration and CIAO² implementations and produced event lists containing the proper grating dispersion coordinates. The spectral extraction was performed using CIAO tools and we also used custom software for some of the broad band spectral analysis. The modeling of the spectra and its lines was done using ISIS³, the emission measure distribution was calculated as in Huenemoerder, Canizares, & Schulz (2001). As already described in paper I, the Orion Trapezium is embedded in a cluster of fairly bright sources. We thus have to clean each spectrum from contributions of interfering cluster sources, which would imitate lines by coincidence, as well as from dispersed photons of other grating spectra crossing the dispersion track of interest. In our cases of interest the latter effect was entirely eliminated by the energy discrimination by the CCDs. Figure 1 shows the HETGS focal plane view near the zeroth order. In both exposures at the top and bottom part of the figure

²<http://chandra.harvard.edu/CIAO2.3>

³<http://space.mit.edu/ISIS>

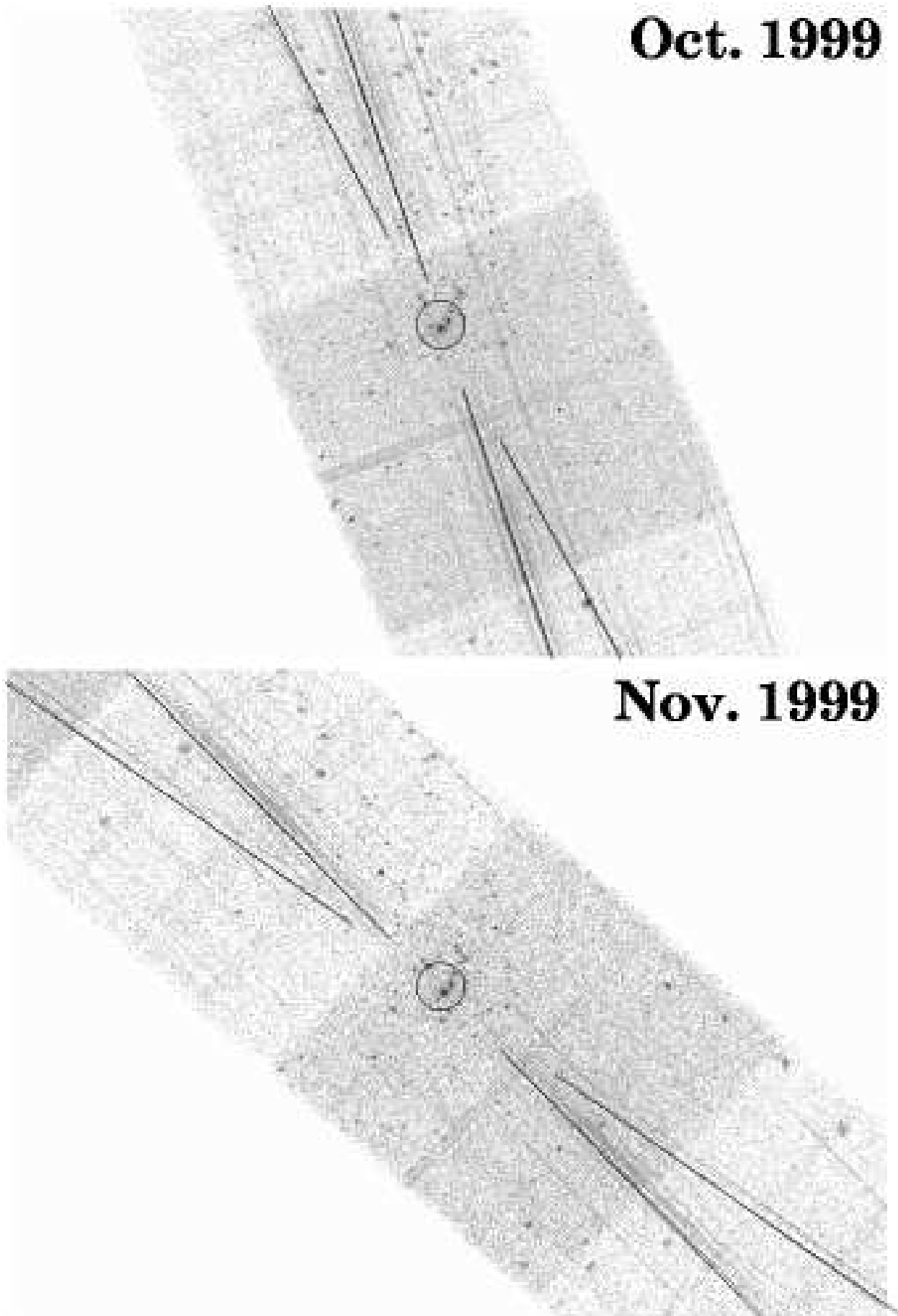


FIG. 1.— Close-up view of the focal plane image near the zeroth order of the HETGS. The top exposure shows the observation from October 1999, the bottom exposure the one from November 1999, which was performed at a different roll angle. Sky north is up, east is left in both images.

we encircled the zeroth order positions of the main Trapezium stars. We also highlighted (for illustration purposes only) the tracks of the dispersed spectra for the brightest source Θ^1 Ori C.

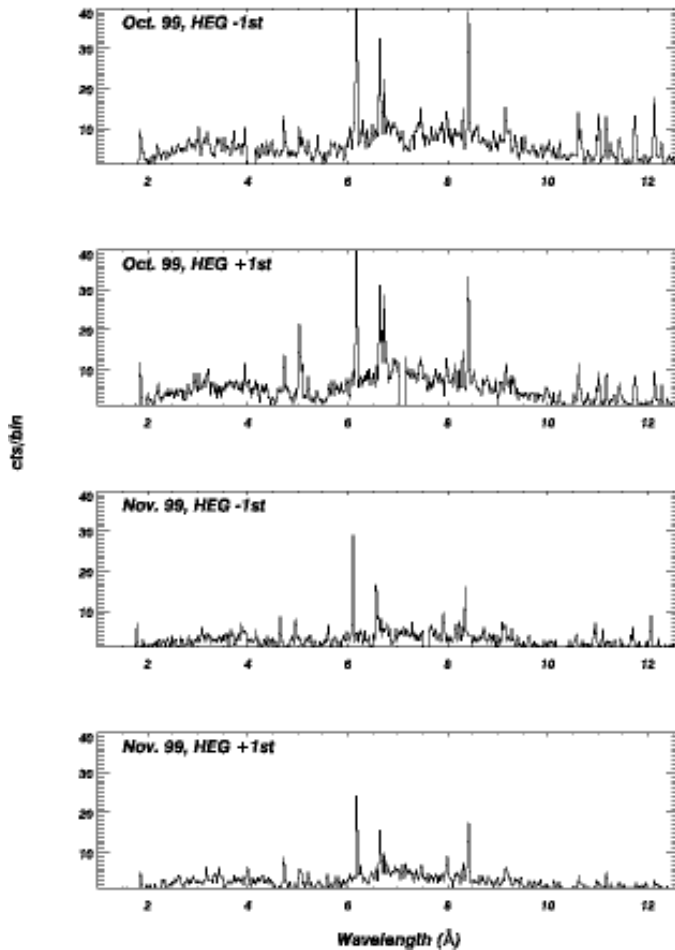


FIG. 2.— HEG 1st order spectra of Θ^1 Ori C. The top two panels show the +1st and -1st spectrum of the first observation, the bottom two panels the same for the second observation.

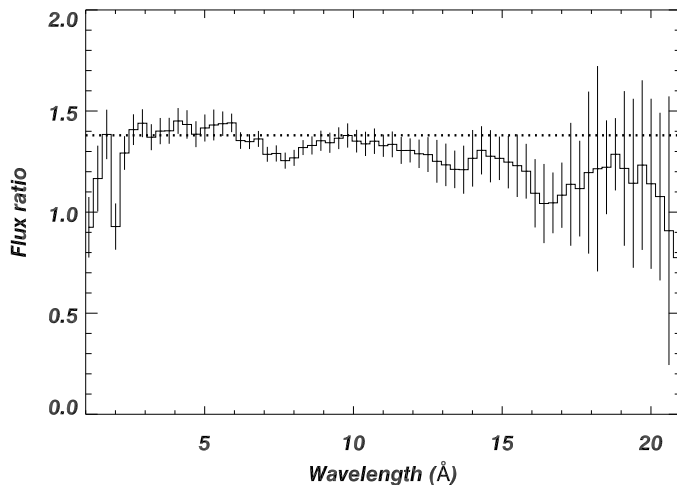


FIG. 3.— The ratio of highly binned (0.5 \AA) and smoothed versions of the co-added spectra from the first and second observation, which correspond to a wind-phase difference of approx. 0.45 in Θ^1 Ori C.

Many spectral tracks from various Trapezium Cluster stars

are detected together with point sources at different off-axis positions which scatter throughout the entire array. One of the differences to the extraction procedure outlined in paper I is that we now have to also extract the spectra of Θ^1 Ori A and E, which have a separation of a few arcsec only and are thus more likely to interfere with each other. We make extensive use of the fact that we have observations at two different roll angles, which gives very good separation at least at one roll angle. Besides visual inspection, we also use the fact that we know the relative fluxes of the two sources from the 0th order CCD spectra. In order to minimize the effect of interfering point sources and parallel dispersion tracks of close sources we sometimes narrowed the cross-dispersion selection range. The standard selection range in cross-dispersion engulfs 95% of the flux and in cases where we narrowed this range we have to re-normalize the fluxes. However we note that by correcting for the expected cross-dispersion profile, we add some systematic errors once we adjust final fluxes. We also correlated detected source point spread functions with the dispersion tracks of the three targets and eliminated the data in the case of a true interference.

2.2. Raw and Exposure Corrected Spectra

Figure 2 shows the first order HEG spectra of Θ^1 Ori C for both observation periods after all cleaning cycles. The weaker appearance of the November 1999 spectra compared to the October 1999 spectra is mostly due to the difference in exposure, but for some lines there may also be variability related to the 15.4 day wind cycle. Here the October observation corresponds to phase 0.82, the November observation to phase 0.37 using the ephemeris from Stahl et al. (1996). In order to investigate this effect we added spectra from the MEG and HEG and divided the exposure corrected flux spectra of the two phases. This spectral ratio is shown in Figure 3. We smoothed and binned the spectra into large (0.5 \AA) bins. The ratio shows that there is a flat part about 38% above unity below 6 \AA . The detailed analysis below shows that the changes are due to variable emissivity at high temperatures. The mean (rms) difference across the whole band is about 24%. Schulz et al. (2001) report different fluxes in the zeroth of about 10%, which is consistent given the uncertainties in that observation due to a over 20% pile up fraction.

2.3. Line Widths

A controversial issue in paper I (see erratum in Schulz et al. 2003) was the analysis of the line widths in the case of Θ^1 Ori C. Due to a software error the line width presented in that paper did not properly account for the response of the instrument and, specifically between 10 and 12 \AA underestimated the amount of line blends. Thus the lines appeared wider than they really are. Here we present the analysis that properly includes the instrument response and takes care of all the line blends. The lines below about 13 \AA clearly appear unresolved. Figure 4 (top) shows lines from three high energy H-like ions, from S XVI, Si XIV, and Mg XII. We chose these lines because they are most likely not affected by blends. The model used for the line fits is described in section 3.2.2 and it fits not only the local but the overall broad band continuum. Thus the model for all three lines comes from the same fit (Figure 4 bottom). Shown are the co-added spectra and models (red curves). In addition we show a broad stretch from the same model fit between 10.5 and 12 \AA showing many highly ionized and blended Fe states. The model sufficiently describes these blends with no

intrinsic broadening. For unresolved lines we can set a 90% confidence limit of the HWHM of 110 km s^{-1} on average based on the statistical properties of the spectrum.

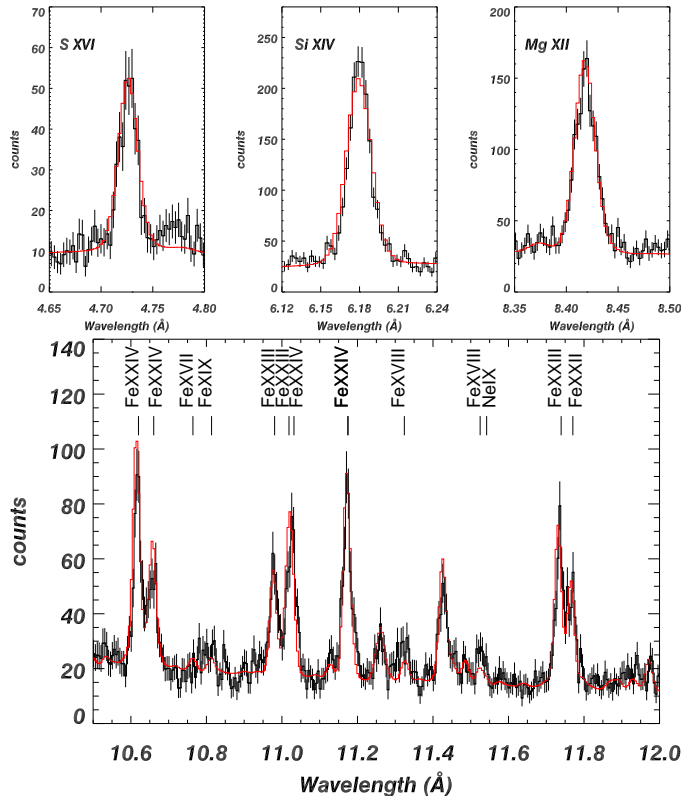


FIG. 4.— **Top:** Model fits of three unblended H-like lines. The red curve is the model (as described in section 3.2.2). HEG and MEG data have been co-added, which allows to oversample to profile with spectral bins of 0.003 \AA . **Bottom:** The same model and spectrum in the wavelength range between 10.5 and 12.0 \AA . It shows a critical stretch of blended Fe lines. The model includes has zero broadening in the lines.

There is a second population of lines at longer wavelengths which are resolved. The statistical quality for many of them is marginal as in this bandpass the spectrum is effectively absorbed. Figure 5 shows the two brightest resolved lines, one from an Fe XVII ion at 15.01 \AA and the O VIII line at 18.97 \AA . The Fe XVII can be fit with a HWHM of 460 km s^{-1} , the O VIII line with a HWHM of 850 km s^{-1} . The latter is also the only one we find slightly blueshifted by about 240 km s^{-1} . In general it is expected to resolve lines better at higher wavelengths since the FWHM is constant with wavelength. However these velocities exceed the confidence limit of 110 km s^{-1} for the unresolved lines considerably and this indicates intrinsic broadening for some lower ionization states.

3. SPECTRAL ANALYSIS

We divide the analysis of the $\Theta^1 \text{ Ori C}$ spectrum into two parts: we model the broad band spectrum with various temperature components of hot plasmas, and we construct an emission measure distribution from single line emissivities. For the latter we need a large number of significant line fluxes, which we only have available in the case of $\Theta^1 \text{ Ori C}$. For the other hot stars we then compute variations of the broad band plasma model derived from the $\Theta^1 \text{ Ori C}$ spectrum.

⁴<http://hea-www.harvard.edu/APEC>

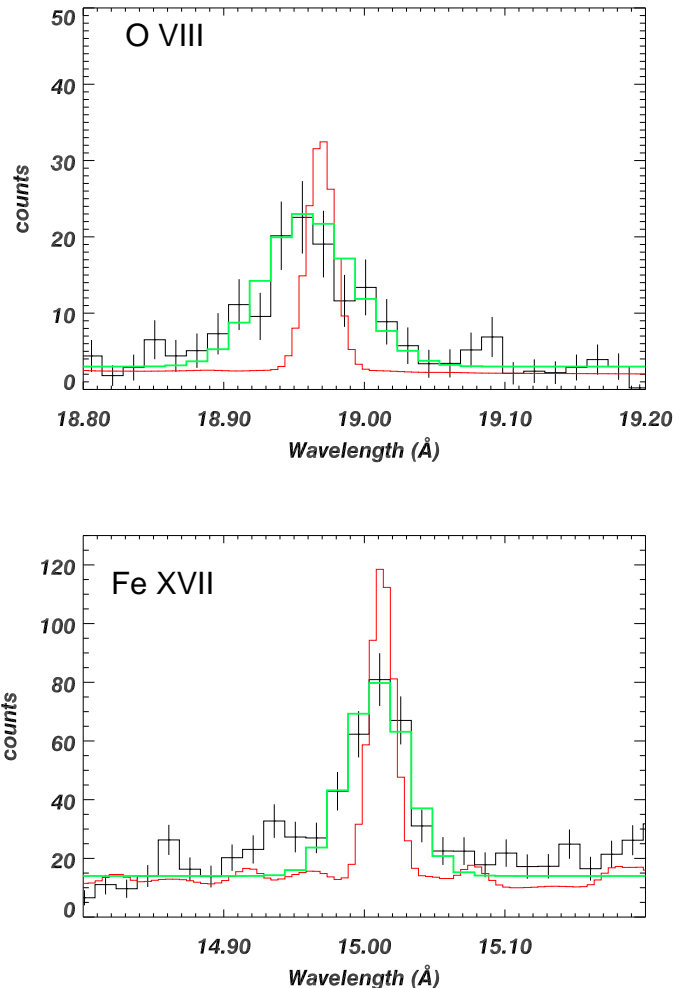


FIG. 5.— The two most significant soft lines in the spectrum. The red line shows the model used in Figure 4 with zero line broadening. The green line is a local Gaussian fit to the data. A comparison shows that both lines appear resolved and show significant broadening. The O VIII in the top diagram also appears blue-shifted.

3.1. The Spectral Model

For the spectral modeling we exclusively use the Astrophysical Plasma Emission Code and Database (APEC and APED⁴) described by Smith et al. (2001). The database is available in ISIS and we can compute emissivities for a collisionally ionized equilibrium plasma in terms of temperature, density, and various abundance distributions. In paper I we deduced that these spectra require a range of temperatures. For the model we assume that all emitting plasmas contributing to the spectrum are in collisional ionization equilibrium. This means that a thermal plasma is in a stable ionization state under the coronal approximation. In this approximation it is assumed that the dominant processes are collisional excitation or ionization from the ground state balanced by radiative decay and recombination. Photo-ionization and -excitation as well as collisional ionization from excited states are assumed to be negligible. Note that due to the usually quite strong UV radiation field near the stellar surface this assumption is not quite true and the meta stable forbidden lines in the He-like triplets may be affected. We will discuss the He-like triplets in a separate section.

From over 80 significant lines we calculate a differential emission measure (DEM) distribution for the two phases separately and for the phase averaged spectra. In the other two stars,

lines in the 10 to 12 Å region, but very strong Fe XXV and still strong lines from other high Z elements. Most important is the existence of a strong continuum. This continuum as well as its high energy cut-off value increases with temperature. The value of this cutoff in connection with the Fe XXV emissivity is a sensitive benchmark for the high temperature of the plasma. The continuum also allows measurements of abundances relative to H, since it is dominated by thermal bremsstrahlung. O VIII (Lyman α at 19 Å) is contributing at all temperatures, at higher temperatures the Lyman β and γ lines become strong as well.

3.2. Θ^1 Ori C

We assumed a line-of-sight column density of 1.93×10^{21} cm⁻² throughout the entire observation. From the measured color excess of $E_{B-V} = 0.32$ (Bolin&Savage 1981) and using the correlation between N_H and E_{B-V} derived from L_α measurements in hot stars by Savage & Jenkins 1972 we expect 1.7×10^{21} cm⁻²; from Spitzer (1978) we expect 1.9×10^{21} cm⁻²; from Predehl & Schmitt (1995) we expect 1.4×10^{21} cm⁻² for the average interstellar medium ($R_v = 3.1$) and 2.4×10^{21} cm⁻² for dense molecular clouds ($R_v = 5.1$). From these numbers an additional opacity in the star cannot be concluded.

3.2.1. Emission Measure Distributions

The procedure for the DEM derivation from an X-ray spectrum is described in Huenemoerder, Canizares, & Schulz (2002). The volume emission measure (VEM) is the volume integral over the product of electron (n_e) and hydrogen (n_H) densities at a given temperature (note: since the emissivity of most emission lines are only weakly dependent on n_e in the expected temperature and density regime, we can as well ignore it). We define a temperature grid of 60 points spaced by 0.05 in log T. The DEM is the derivative of the volume emission measure with respect to log T. It incorporates the emission measure and abundance of many ions and reflects the energy balance of the plasma with respect to temperature.

In Table 1 we show the list of detected lines with measured and predicted line positions and fluxes for the combined spectra. We also, using APED, computed a temperature of maximum emissivity from each ion. The tables are sorted by ion species, which approximately reflects temperature as well.

The first part of Table I shows lines from all Fe ions accepted by the fit with one σ confidence errors for the line fluxes. It is specifically remarkable to see a large number of ion states larger than Fe XXII, specifically Fe XXIV, and ion states lower than XIX, specifically Fe XVII. The fractional abundances (i.e. the ratio of integrated flux of a specific ion species over all Fe emission) show a dominance of Fe XXIII to Fe XXV ions (0.36) as well as Fe XVII to Fe XIX (0.58), but a significant lack of Fe XX to XXII ions (0.06). The line positions agree well within the expected uncertainties with the positions produced by APED. The second part of Table I shows the list of ions with Z lower than 26. The results are very similar to what we observe for Fe ions, i.e. lines from low and high temperatures dominate the fractional abundances.

Figure 7 (top) shows the DEM versus temperature over a range from 3 to 300 MK. The middle (red) line shows the distribution, the upper and lower lines (green) trace the 90% uncertainty range. There are clearly three peaks visible at 7.9 ± 0.2 MK, 26.3 ± 1.8 MK, and 66.1 ± 11.2 MK. The emissivity is dominated by plasmas at temperatures higher than 15 MK

with a temperature tail that allows the distribution to exceed 100 MK. There is a prominent gap at 7.15 MK that divides the DEM into emission from high and low temperature plasmas. This drop roughly corresponds to the missing emissivities from Fe XX to XXII ions in Table 1. The low temperature peak incorporates most ions from O to Si and Fe XVII to Fe XXII, while the high temperature DEM corresponds to Fe XXIII to Fe XXV, Si to Ca. There is also an incision in the high temperature part of the DEM that roughly corresponds to the weak showing of S XVI and Ca XIX in one of the spectra (see below).

The middle part of Figure 7 show the DEMs for two phases separately. The solid lines show the upper and lower error limits of the DEM for phase 0.82, the dotted lines the same for phase 0.37. There are a few remarkable characteristics. The incision between high and low temperature at 7.15 MK persists in both phases and the low temperature emissivity is similar. The high temperature emissivity shows a significant difference in that the middle peak is much more pronounced in phase 0.82 whereas the high temperature peaks appear unchanged. This means the overall variability in line emissivity is predominately in the Fe XXII and Fe XXIV lines as well as in the Si XIV, where we observe the bulk of the emissivity.

The DEM fit also adjusts abundances (bottom of Figure 7) with respect to solar abundances. Here we find for Mg, Si, S, Ar, Ca ions no significant deviation from solar values. For O we find a factor of 0.2 ± 0.1 , for Ne and Fe a factor of 0.5 ± 0.1 underabundance. We find this distribution in both observations. Additional uncertainties in these values may stem from uncertainties in the ionization balance (Mazzotta et al. 1998). However we also have to stress the point that once we apply the spectra for each ion fitted in the DEM analysis we find a sufficient fit to the total spectrum (see also below).

The determination of the continuum in the DEM analysis is an iterative process assuming that all continuum contributions come from the same thermal plasma generating the emission lines. Contributions from a non-thermal component critically affect the Fe abundances. A predicted shape of $\propto E^{-1/2}$ of a Compton component (Chen and White 1991) most prominently contributes to the continuum near the Fe XXV line. However the continuum level there is already quite determined by the fits to the Fe XXIV lines and their adjacent continuum levels. We estimate that the contribution cannot be more than about 1% to the total X-ray flux.

3.2.2. Phase-averaged Plasma Model

Figure 8 shows the phase averaged count spectrum binned by 0.005 Å. MEG and HEG have been added. In this approach we model this spectrum with a few constrained components by approximating the emission measure above. This section in this respect does not produce much new information, but verifies the method used for the fainter stars. However, for reasons of consistency we use the luminosities and fluxes determined in this section for further discussion. We rebin the above DEM into a few coarse intervals and calculate a model component for each DEM interval. We could calculate the model directly from each DEM bin, i.e. from the log T (K) = 0.05 grid. However the idea is to produce a simplified model in good approximation to the DEM. The models were again calculated using the APED database, folded through the spectral response function and were then fit to the measured spectra.

TABLE 1 FE IONS DETECTED IN Θ^1 ORI C

ion	$\langle \log T \rangle$ K	λ_o Å	λ_{maes} Å	flux 10^{-5} ph s $^{-1}$ cm $^{-2}$
Fe XXV	7.8	1.860	1.858	7.534± 1.225
Fe XXIV	7.4	7.169	7.170	1.341± 0.252
Fe XXIV	7.4	7.996	7.989	1.774± 0.232
Fe XXIV	7.4	8.316	8.233	0.884± 0.200
Fe XXIV	7.4	8.233	8.285	0.248± 0.177
Fe XXIV	7.4	8.285	8.304	0.924± 0.348
Fe XXIV	7.4	10.619	10.620	5.825± 0.585
Fe XXIV	7.4	10.663	10.660	3.453± 0.494
Fe XXIV	7.4	11.029	11.032	3.359± 1.209
Fe XXIV	7.4	11.176	11.175	7.026± 0.718
Fe XXIII	7.2	8.304	8.316	1.484± 0.364
Fe XXIII	7.2	8.815	8.816	1.139± 0.243
Fe XXIII	7.2	10.981	10.981	3.029± 0.456
Fe XXIII	7.2	11.019	11.019	2.592± 0.000
Fe XXIII	7.2	11.736	11.739	5.927± 0.693
Fe XXIII	7.2	12.161	12.160	3.388± 0.950
Fe XXII	7.1	8.975	8.974	0.561± 0.224
Fe XXII	7.1	11.770	11.771	4.141± 0.602
Fe XXI	7.1	12.284	12.286	4.355± 0.908
Fe XX	7.0	9.219	9.194	1.151± 0.272
Fe XX	7.0	14.267	14.248	0.614± 0.667
Fe XIX	6.9	10.816	10.814	0.862± 0.307
Fe XIX	6.9	13.462	13.460	3.366± 0.970
Fe XIX	6.9	13.497	13.490	3.536± 0.950
Fe XIX	6.9	13.518	13.520	5.639± 1.157
Fe XIX	6.9	15.079	15.086	2.156± 1.182
Fe XIX	6.9	16.110	16.098	1.637± 1.006
Fe XVIII	6.8	11.326	11.324	1.433± 0.372
Fe XVIII	6.8	11.527	11.525	1.532± 0.521
Fe XVIII	6.8	14.208	14.208	3.472± 1.057
Fe XVIII	6.8	14.256	14.268	0.943± 0.626
Fe XVIII	6.8	14.534	14.535	1.493± 0.658
Fe XVIII	6.8	16.071	16.071	4.501± 1.445
Fe XVIII	6.8	16.159	16.184	1.100± 0.804
Fe XVII	6.8	10.770	10.764	0.565± 0.289
Fe XVII	6.7	12.124	12.129	8.754± 1.168
Fe XVII	6.7	12.266	12.265	2.184± 0.580
Fe XVII	6.7	15.014	15.014	18.463± 2.347
Fe XVII	6.7	15.261	15.261	5.316± 1.181
Fe XVII	6.7	16.780	16.775	10.039± 2.255
Fe XVII	6.7	17.051	17.051	8.044± 2.099
Fe XVII	6.7	17.096	17.095	6.147± 1.921

TABLE 1 CONT.: LOWER (< 26) Z IONS

ion	$\langle \log T \rangle$ K	λ_o Å	λ_{maes} Å	flux 10^{-5} ph s $^{-1}$ cm $^{-2}$
Ca XX	7.8	3.024	3.024	0.602± 0.285
Ca XIX	7.5	3.177	3.179	1.206± 0.326
Ca XIX	7.5	3.207	3.209	0.752± 0.292
Ar XVII	7.4	3.365	3.372	0.303± 0.325
Ar XVIII	7.7	3.731	3.735	1.002± 0.359
Ar XVII	7.4	3.949	3.943	1.695± 0.380
Ar XVII	7.3	3.966	3.960	1.243± 0.489
S XVI	7.6	4.733	4.729	5.327± 0.619
S XV	7.2	5.039	5.039	5.201± 0.710
S XV	7.2	5.067	5.065	1.798± 0.486
S XV	7.2	5.102	5.100	2.378± 0.541
Si XIV	7.4	5.218	5.217	2.394± 0.510
Si XIV	7.4	6.180	6.181	11.662± 0.562
Si XIII	7.0	5.681	5.684	0.836± 0.276
Si XIII	7.0	6.648	6.648	7.432± 0.472
Si XIII	7.0	6.687	6.686	2.515± 0.328
Si XIII	7.0	6.740	6.740	3.717± 0.342
Al XII	7.0	7.757	7.760	0.595± 0.196
Al XII	6.9	7.872	7.874	0.256± 0.184
Mg XII	7.2	7.106	7.105	1.554± 0.235
Mg XI	6.9	7.850	7.850	0.747± 0.206
Mg XII	7.2	8.419	8.420	8.406± 0.484
Mg XI	6.8	9.169	9.168	3.085± 0.370
Mg XI	6.8	9.231	9.230	1.966± 0.314
Mg XI	6.8	9.314	9.310	0.917± 0.305
Ne X	7.0	9.481	9.478	1.351± 0.271
Ne X	7.0	9.708	9.710	0.889± 0.250
Ne X	7.0	10.240	10.240	1.822± 0.334
Ne IX	6.6	11.544	11.542	0.595± 0.454
Ne X	6.9	12.132	12.144	5.325± 1.131
Ne IX	6.6	13.447	13.435	3.804± 0.995
Ne IX	6.6	13.550	13.550	3.827± 0.962
O VIII	6.7	14.821	14.840	0.930± 0.622
O VIII	6.7	15.176	15.195	2.767± 0.910
O VIII	6.7	16.006	16.010	3.934± 1.200
O VII	6.4	18.627	18.635	4.067± 2.007
O VIII	6.7	18.973	18.970	21.143± 3.008
O VII	6.3	21.602	21.600	10.230± 5.583
O VII	6.3	21.804	21.799	10.451± 5.991

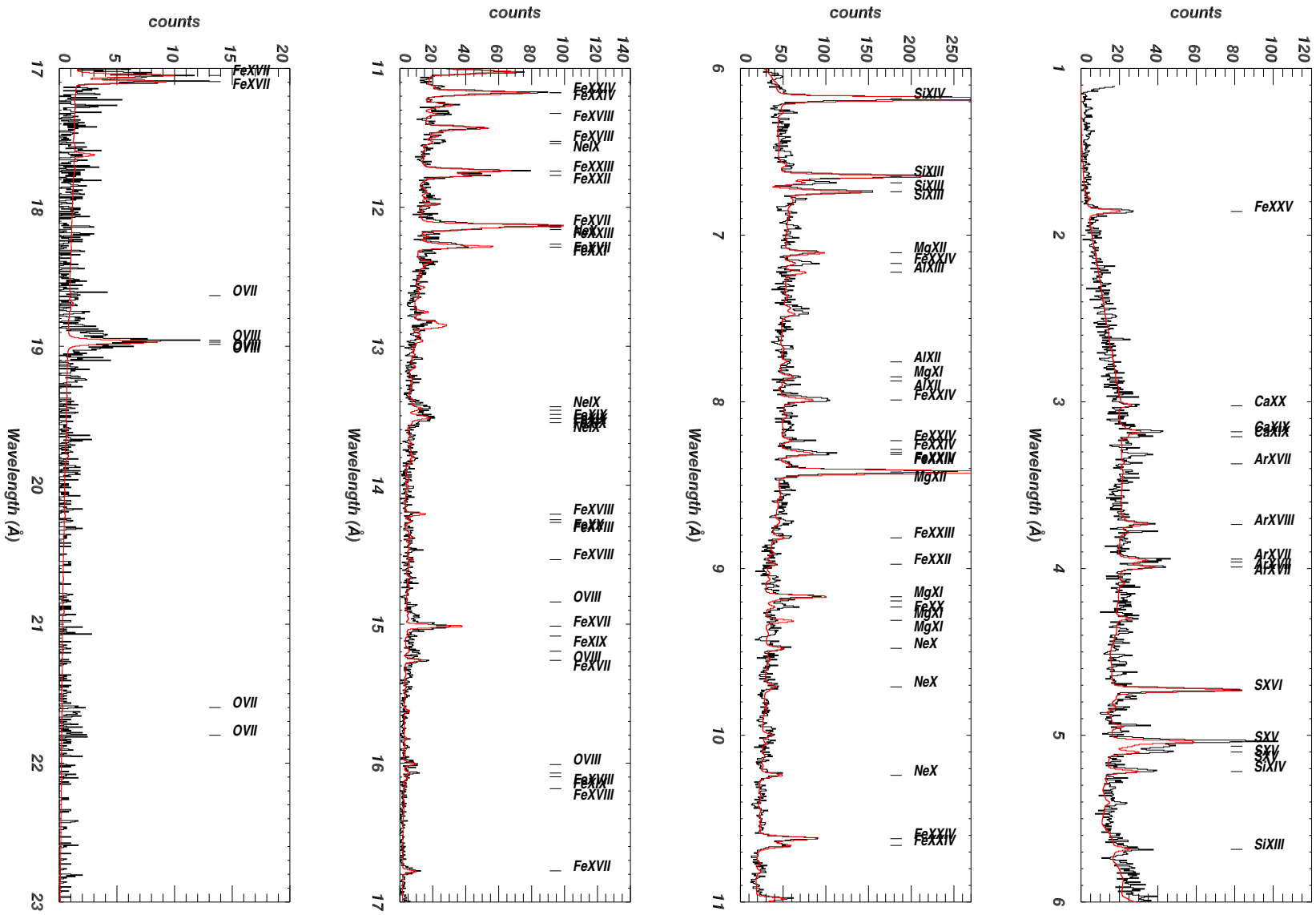


FIG. 8.— The measured phase averaged count spectrum over the full exposure for Θ^1 Ori C. The bins of the spectrum have a value of 0.005 \AA . The red line is the approximated phase-averaged plasma model deduced for this spectrum.

TABLE 2 TEMPERATURE COMPONENTS FROM MODEL FITS

star	comp. #	log T K	norm erg s ⁻¹ cm ⁻²	L _x (1-10 keV) erg s ⁻¹
Θ ¹ Ori C	1	6.79±0.06	6.55×10 ⁻¹³	7.93×10 ³⁰
	2	6.97±0.07	2.22×10 ⁻¹²	2.69×10 ³¹
	3	7.22±0.07	1.24×10 ⁻¹²	1.50×10 ³¹
	4	7.47±0.08	4.62×10 ⁻¹²	5.60×10 ³¹
	5	7.64±0.06	2.51×10 ⁻¹²	3.04×10 ³¹
	6	7.82±0.07	5.20×10 ⁻¹²	6.30×10 ³¹
Θ ¹ Ori E	1	6.63±0.08	1.55×10 ⁻¹³	1.87×10 ³⁰
	2	7.02±0.08	3.78×10 ⁻¹³	4.60×10 ³⁰
	3	7.31±0.07	4.88×10 ⁻¹³	5.92×10 ³⁰
	4	7.49±0.06	1.85×10 ⁻¹³	2.23×10 ³⁰
	5	7.67±0.06	1.31×10 ⁻¹²	1.59×10 ³¹
Θ ¹ Ori A	1	6.68±0.09	3.41×10 ⁻¹⁴	4.13×10 ²⁹
	2	7.06±0.08	3.54×10 ⁻¹³	4.29×10 ³⁰
	3	7.34±0.08	1.08×10 ⁻¹³	1.31×10 ³⁰
	4	7.48±0.07	4.28×10 ⁻¹³	5.18×10 ³⁰
	5	7.63±0.07	2.76×10 ⁻¹³	3.35×10 ³⁰

We fit only one component at a time (keeping the parameters of the other ones fixed) and repeated this step with the other components until the final spectrum meets the criteria below. To sensitively constrain the model we use the DEMs above, which helps us to constrain the relative strengths of the components: the level of the continuum, the position of its high-energy cut-off, the strength of the Fe XXV lines and various temperature dependent line ratios.

Our model reproduces all major properties of the spectrum. There are several small deviations relating to the fact that the model cannot yet reproduce all subtle details. The results are summarized in Table 2. The stated temperature uncertainties are large which is a consequence of the large error envelopes of the DEM in combination with a now very coarse temperature grid. The stated fluxes and luminosities have errors between 5 and 15%. Several key properties in the spectrum are well modeled: the total flux derived from the model and from the exposure corrected data in the range of 1 to 25 Å agree within 2%, the continuum is well represented and the line ratios agree within 10%.

The final result is overplotted in Figure 8. The thermal flux continuum shows a cut-off around 3.4 Å. In order to get this cut-off we need a high temperature of 66.5 MK. The shallow decline of the continuum below the cut-off requires stronger intermediate temperature components (43.8 and 29.5 MK), which are constrained by by line ratios of Si, S, and Fe lines as well as the fact that the sum of the Fe XXV line fluxes of these two high temperature components need to match the observed line flux. These three components account for almost all of the continuum providing 75% of the star's X-ray luminosity. The low temperature components at 6.1, 9.3 and 16.5 MK produce many lines between 9 and 20 Å but account only for a fraction of the total luminosity. In fact, if the star did not have hot components, it would be faint. From Table 2 the X-ray luminosity accounting for the low temperature DEM component only is 3.5×10^{31} erg s⁻¹. Using the bolometric luminosity as listed by Berghöfer, Schmitt, and Cassinelli (1996) we find -7.2 for the low temperature log L_x/L_{bol} . More than 85% of the luminosity is radiated by plasmas with temperatures higher than 1.5×10^7 K, and 75% from temperatures higher than 3×10^7 K. This is consistent with the results from the zero order CCD spectra (Schulz et al. 2001). The abundances had to be adjusted during the fit as well and the result is similar to the distribution observed in the DEM analysis.

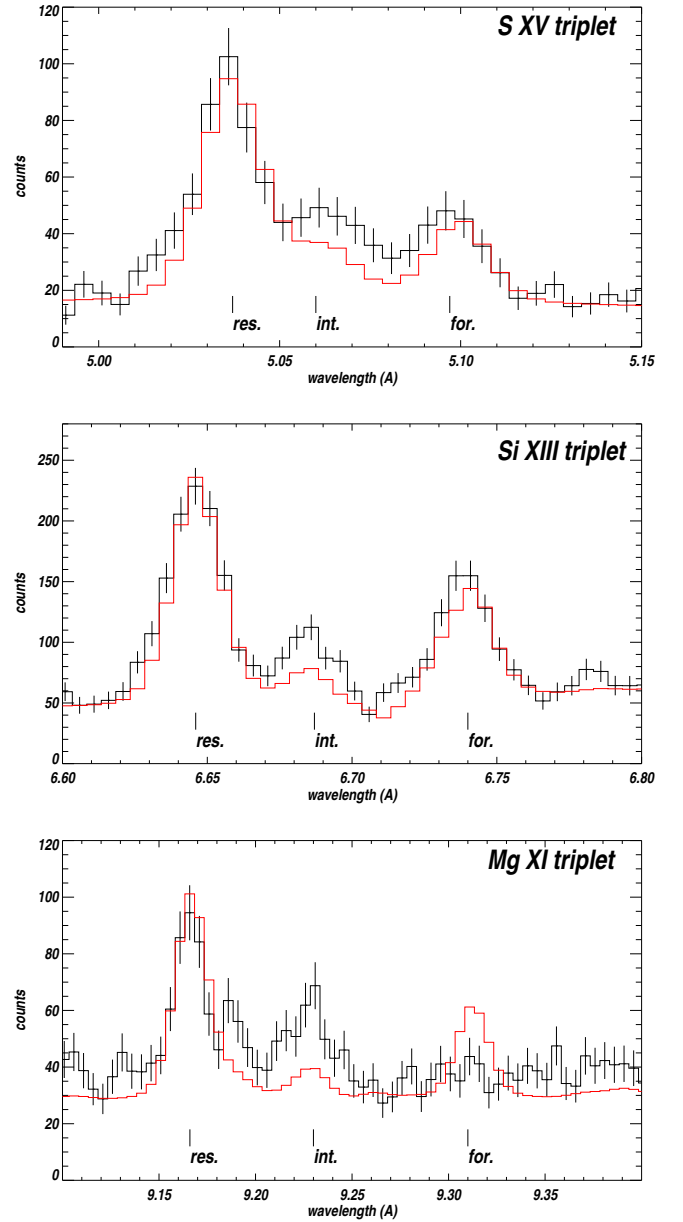


FIG. 9. — The He-like triplets from S (top), Si (middle), and Mg (bottom) from the spectrum in figure 8. The model here has been optimized such for each triplet that it fits the recombination line.

3.2.3. Optical depths, Formation Radii and Densities

Line ratios may be used to place limits on optical depths, line formation radii and densities. Schmelz, Saba, and Strong (1992) suggested that the Fe XVII (upper-level $2p^5 3d^1 P_1$) line at 15.01 Å could be used as a measure for resonant scattering (and thus density) in the emitting plasma. Specifically the ratio to its Fe XVII resonance line neighbor at 15.26 Å ($2p^6 \ ^1S_0 - 2p^5 3d^3 D_1$) is of interest (see also Waljeski et al. 1994, Brickhouse et al. 2000 and a discussion in Huenemoerder, Canizares, and Schulz 2001). From the APED database we deduce a theoretical ratio of 3.57 for the optically thin limit. The measured ratio in the spectrum is 3.47 ± 1.21 and thus despite the large error bar indicates agreement with a low density plasma. The formation radius of this line can be estimated from its line width. This line was indeed resolved with a HWHM of 460 km s⁻¹. The standard law of velocity for the acceleration zone of the wind $v(r) = v_\infty (1 - r_{star}/r)^\beta$ (Lamers & Cassinelli 1999) with

the index $\beta = 0.88$ and a terminal velocity of 1000 km s^{-1} would then locate the line emitting region to slightly more than half a stellar radius from the photosphere.

Another line that was resolved was the O VIII line at 18.97 \AA . Its HWHM corresponds to velocity of 850 km s^{-1} , which would place the emitting region almost near the terminal velocity of the wind at about 7 stellar radii from the photosphere. In contrast, the line width limit of 110 km s^{-1} would place the emitting radius of all the other (non He-like) lines to within 10% of a stellar radius above the photosphere (see also Cohen et al. 2002 for $\tau \text{ Sco}$). Whether there should be an asymmetry of the line due to occultation seems irrelevant since we do not resolve most of the lines.

The forbidden lines in the He-like triplets are meta-stable and their ratio with the corresponding intercombination lines is density sensitive above some ion-dependent threshold. Figure 9 shows the observed He-like triplets from S XV, Si XIII, and Mg XI. The model fits for these triplets have been optimized for each element to specifically fit the resonance line. One of the most striking effects seen in the triplets from O VII (very faint), Ne IX, and Mg XI (Figure 9, bottom) is that the forbidden line is not observed, while it still appears quite prominent in Si XIII and S XV (Figure 9 middle and top). Although the forbidden transition in the Si XIII triplet is blended with the Lyman γ line of Mg XII, based on the flux observed in the Mg XII Lyman α line, the Lyman γ contribution cannot be more than 5%. However we observe a forbidden line flux comparable to the expectation of the model. We observe a similar picture in S XV (which is not blended), however the f/i ratio here is not sensitive to densities lower than 10^{14} cm^{-3} .

All the triplets are subject to UV excitation and it has been shown by Kahn et al. (2001) (see also Blumenthal, Drake, and Tucker 1972) in the example of $\zeta \text{ Pup}$ that the low f/i ratios in line driven wind plasmas are not likely an effect of collisional excitation in high density plasmas, but rather are due to the destruction of the forbidden line by the large UV flux at the corresponding excitation wavelengths. Waldron and Cassinelli (2001), Cassinelli et al. (2001) and Miller et al. (2002) use model UV fluxes (e.g. Chavez, Stalio, and Holberg 1995) to estimate radial constraints on the X-ray emitting plasma. Such an analysis in the case of $\Theta^1 \text{ Ori C}$ is highly delicate. One critical item is the modeling of the actual UV flux between ~ 900 and 1500 \AA , which provides the source for the photoexcitation in Si XIII, and Mg XI. We checked the ratio of the UV spectra of $\Theta^1 \text{ Ori C}$ and $\zeta \text{ Pup}$ using Copernicus data (Snow & Jenkins 1977) and after correcting for the different stellar parameters ($19 R_{\odot}$, 42500 K , $E_{B-V} = 0.07$ for $\zeta \text{ Pup}$; $8 R_{\odot}$, 39000 K , $E_{B-V} = 0.35$ for $\Theta^1 \text{ Ori C}$; Pauldrach et al. 1994, Howard & Prinja 1989, Berghöfer, Schmitt, and Cassinelli 1996) we could not quite reconcile the model with the data in a sense that the UV flux in $\Theta^1 \text{ Ori C}$ seems lower than the model. A proper correction for extinction is certainly critical.

Effectively there no obvious reason why the UV field should be weaker than one would expect from blackbody model atmospheres (MacFarlane et al. 1993, Chavez, Stalio, and Holmberg 1995). In this respect we estimated the formation radius by assuming a blackbody spectrum of 39000 K for the radiation field for an O7V star (Howard & Prinja 1989) as an upper limit. The surface temperature of $\Theta^1 \text{ Ori C}$ is also a source of uncertainty, as $\Theta^1 \text{ Ori C}$ is classified somewhere between O6 and O7.5, sometimes even as O4. In case of the latter the result can differ by over 60%. We calculated the photoionization (PE)

rates using the recipe provided by Kahn et al. (2001, see also Mewe & Schrijver 1978) and obtained $2^3 S - 1^1 S$ decay rates from Drake (1971). In Mg XI the forbidden line can be only marginally detected above the 1σ error of the continuum and here we consider the radius where the PE rate is of the order of the decay rate as critical. The f/i ratios in Si and S are, though reduced from the one expected from the atomic data in the optically thin limit, significantly larger. Here we have to assume that the formation radius is farther away from the stars surface and the PE rate is correspondingly smaller. Thus for Mg we find an upper limit to the formation radius of 4.2 stellar radii, for Si 2.0 stellar radii and 1.3 stellar radii for S.

On the other hand it should be mentioned that in the case of zero UV flux the f/i ratio of the triplets can also be used as density diagnostics. We then obtain densities of $< 4 \pm 2 \times 10^{13} \text{ cm}^{-3}$ for Mg and $< 9 \pm 8 \times 10^{13} \text{ cm}^{-3}$ for Si, repeating the result stated in paper I.

3.3. $\Theta^1 \text{ Ori E and A}$

The next two X-ray brightest stars in the Trapezium are stars A and E with X-ray fluxes of 1.3 to $2.5 \times 10^{-12} \text{ erg cm}^{-2} \text{ s}^{-1}$ corresponding to luminosities of 2 to $4 \times 10^{31} \text{ erg s}^{-1}$, respectively (Schulz et al. 2001). These fluxes are an order of magnitude fainter than $\Theta^1 \text{ Ori C}$, which is likely due to their B spectral types (Cassinelli et al. 1994). In this respect the HETGS spectra are less brilliant, however in both spectra we are still able to detect quite a number of emission lines and strong continua. This at least allows us to sufficiently constrain our multicomponent model. Table 3 shows the characteristics of the brightest lines for both stars. These line properties are very similar to the characteristics exhibited by $\Theta^1 \text{ Ori C}$. This is specifically noteworthy for the Fe XXIV transitions. The lines appear unresolved in both stars and we can set a HWHM confidence limit of 160 km s^{-1} . In general we observe the same most remarkable features: the strong continuum and very narrow and symmetric lines.

Figures 10 and 11 show the count spectra of the two stars binned to 0.015 \AA . The red solid lines are the final model spectra. We fitted these spectra following the procedure described in section 3.2.2. The result for $\Theta^1 \text{ Ori E}$ is shown in the middle part, for $\Theta^1 \text{ Ori A}$ in the bottom part of Table 3. Both spectra accepted 5 components including a quite marginal low temperature component. The four higher temperature components seem similar to components 2-5 in $\Theta^1 \text{ Ori C}$, with the one for the very high temperature missing. In this respect we observe a similar bifurcation in emissivity in stars A and E, which includes low temperature emissivity below at or below 10^7 K and strong emissivity that has temperatures significantly higher than 10^7 K . In the case of $\Theta^1 \text{ Ori E}$ roughly 80% and for $\Theta^1 \text{ Ori A}$ 70% of the luminosity appears at temperatures higher than $1.5 \times 10^7 \text{ K}$. Over 50% of the luminosity originates from emitting plasmas showing temperatures higher than $3 \times 10^7 \text{ K}$. Thus if we again only count the flux of the low temperature component as the one from the unconfined wind, the ratio $L_x^{\text{wind}}/L_{\text{bol}}$ for these two sources are similar to the one for $\Theta^1 \text{ Ori C}$ and thus consistent with normal O-stars. The fit abundances are also similar to values for $\Theta^1 \text{ Ori C}$, except that the Ne lines are stronger, and we do not detect a deviation from solar values.

Most He-like triplet are too weak to perform a meaningful analysis except for Si XIII, where in the case of star E (Figure 10, 6.74 \AA) we observe a forbidden line that is almost as strong as the resonance line. In star A it is not as strong but clearly

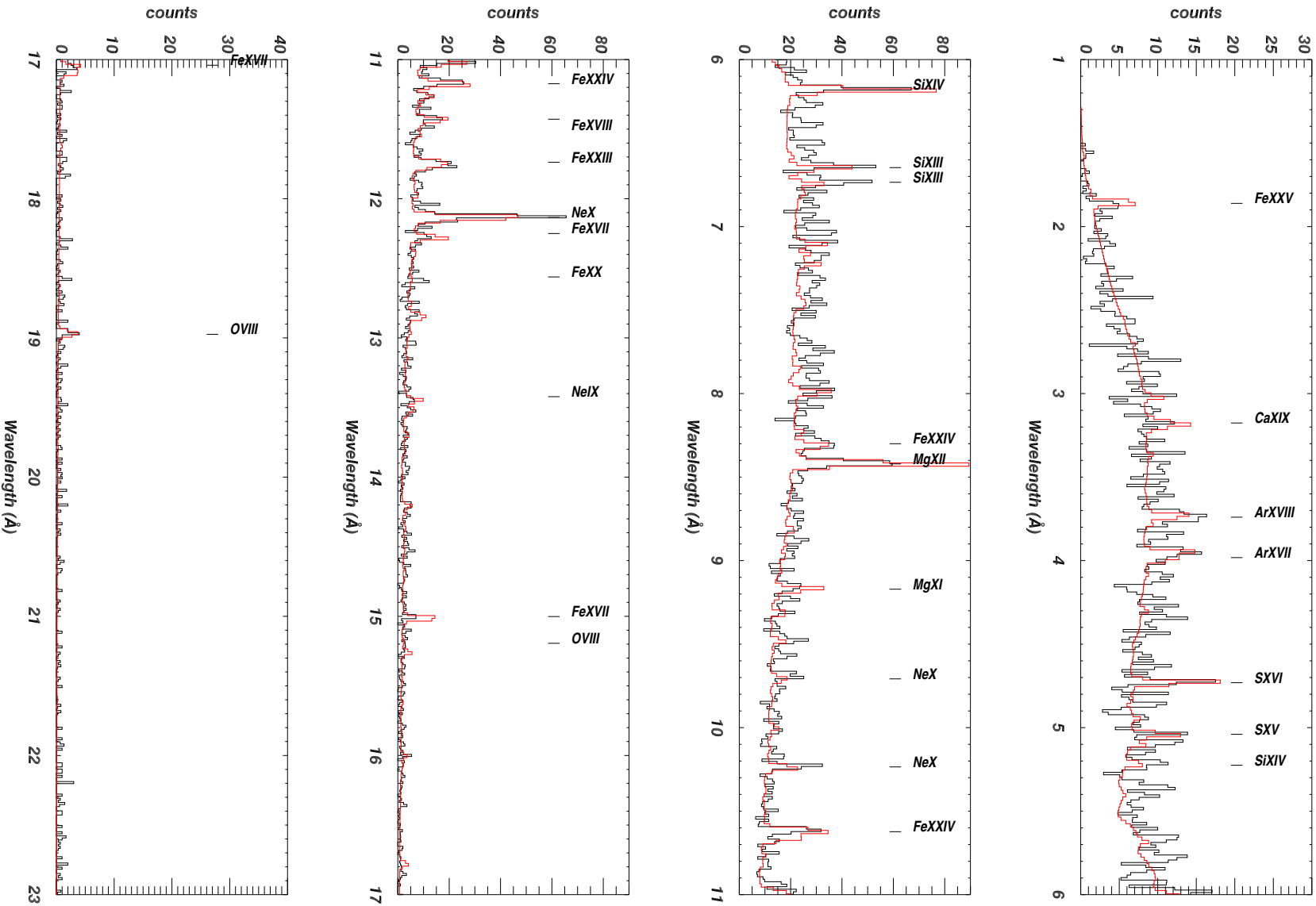


Fig. 10.— The measured count spectrum for Θ^1 Ori E. The red line is the best fit found using a multi temperature APED model

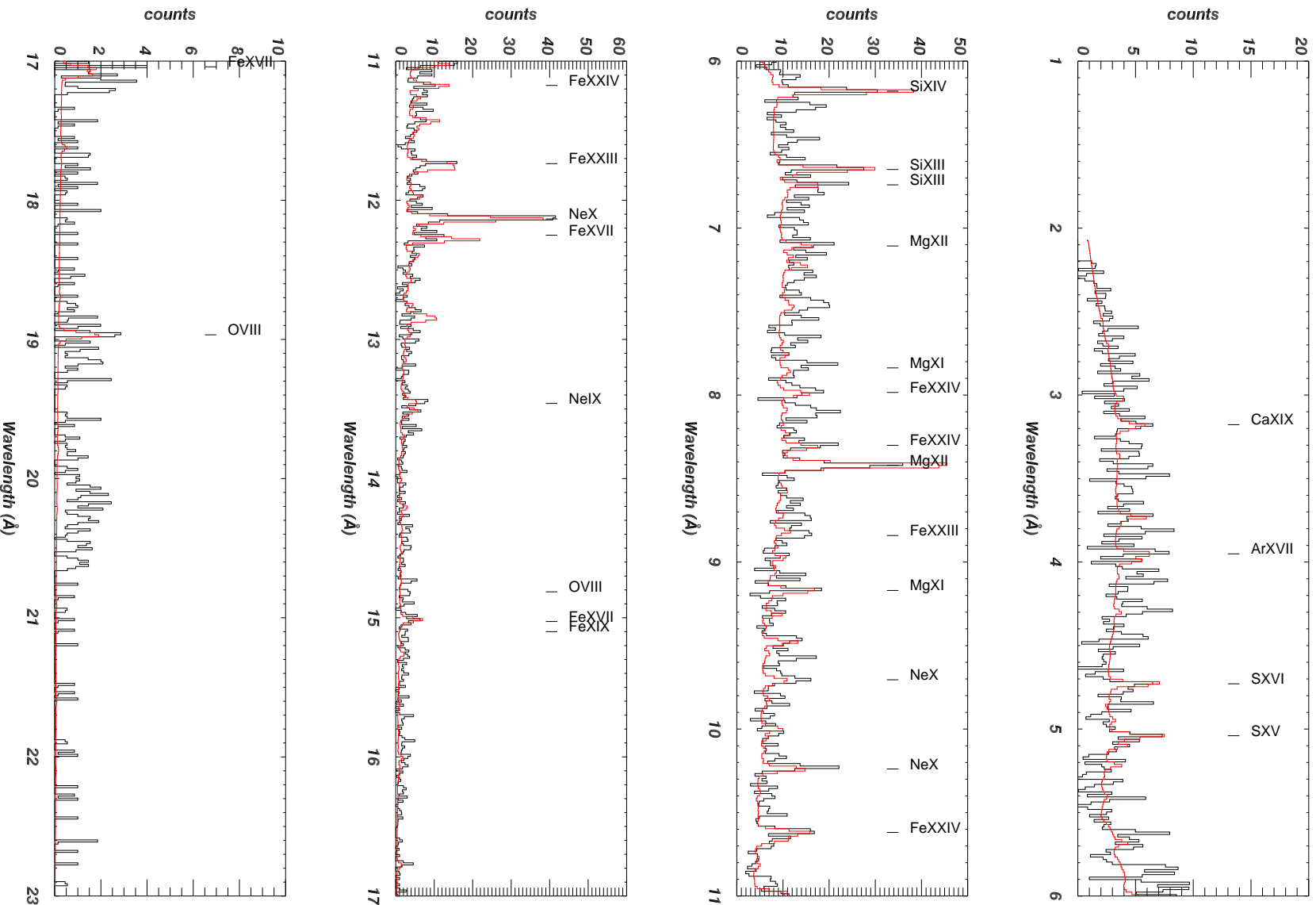


Fig. 1.— The measured count spectrum for Θ^1 Ori A. The red line is the best fit found using a multi temperature APED model

detectable. In both cases we do not detect an intercombination line and by setting a limit to the line using the 1σ error of the continuum we can only get rough estimate of the f/i ratio. We nevertheless we can put some limits on the formation radius of Si XIII. In the optically thin limit without photoexcitation we expect 2.16 for the f/i ratio. For star E we can limit the ratio to 3.43 ± 1.69 , consistent with the then limit and basically no UV destruction. Assuming a B0.5V star with a surface temperature of 23000, we would expect the forbidden line would get completely destroyed within 0.4 stellar radius above the photosphere. Since this is not the case and the line seems to be fully intact, we assume that the 2^3S-1^1S decay rate entirely dominates the PE rate, which should occur at a distance of 1.4 stellar radii. For star A the ratio is 2.13 ± 1.33 we can make the same argument assuming a surface temperature of 20000 K (B1V, Strickland 2000). In terms of density, i.e. under the assumption that there is no photoexcitation, the f/i ratios seem to be in compliance with the densities below 10^{13} g cm^{-3} .

TABLE 3 : IDENTIFIED IONS IN Θ^1 ORI A AND E

ion	λ_o Å	flux (Θ^1 Ori A) $10^{-6}\text{ ph s}^{-1}\text{ cm}^{-2}$	flux (Θ^1 Ori E) $10^{-6}\text{ ph s}^{-1}\text{ cm}^{-2}$
Fe XXV	1.861	-	7.182 ± 1.077
Ca XIX	3.198	0.895 ± 0.134	1.481 ± 0.222
Ar XVIII	3.734	-	3.321 ± 0.498
Ar XVII	3.949	0.298 ± 0.045	2.274 ± 0.341
S XVI	4.730	0.840 ± 0.126	5.233 ± 0.785
S XV	5.039	1.097 ± 0.165	2.737 ± 0.411
Si XIV	5.217	-	1.194 ± 0.179
Si XIV	6.183	3.293 ± 0.494	3.935 ± 0.590
Si XIII	6.648	1.731 ± 0.260	2.573 ± 0.386
Si XIII	6.740	1.706 ± 0.256	2.751 ± 0.413
Fe XXIV	7.989	0.676 ± 0.101	-
Fe XXIV	8.304	0.676 ± 0.101	1.658 ± 0.249
Mg XII	8.420	2.612 ± 0.392	5.060 ± 0.759
Fe XXIII	8.815	1.363 ± 0.204	-
Mg XI	9.169	1.963 ± 0.294	2.495 ± 0.374
Ne X	9.708	0.811 ± 0.122	2.393 ± 0.359
Ne X	10.239	3.078 ± 0.462	3.530 ± 0.530
Fe XXIV	10.619	2.919 ± 0.438	3.508 ± 0.526
Fe XXIII	10.983	-	2.048 ± 0.307
Fe XXIV	11.176	1.013 ± 0.152	4.392 ± 0.659
Fe XXIII	11.736	2.186 ± 0.328	2.875 ± 0.431
Fe XVIII	11.330	-	3.442 ± 0.516
Ne X	12.135	14.589 ± 2.188	16.331 ± 2.450
Fe XVII	12.261	1.558 ± 0.234	0.498 ± 0.075
Fe XX	12.576	-	1.617 ± 0.242
Ne IX	13.445	5.727 ± 0.859	37.722 ± 5.658
Fe XVII	15.014	21.573 ± 3.236	4.164 ± 0.625
Fe XIX	15.079	8.305 ± 1.246	-
O VIII	15.176	-	18.360 ± 2.754
Fe XVII	17.051	5.309 ± 0.796	13.059 ± 1.959
O VIII	18.970	0.177 ± 0.027	9.362 ± 1.404

4. DISCUSSION

High resolution X-ray spectra provide new and more powerful diagnostics of the high energy emission from hot star plasmas. These diagnostics involve line identifications, the relation of specific line ratios with physical parameters such as temper-

ature and density, line shapes and shifts as well as full scale plasma models. In paper I we presented a preliminary line list for Θ^1 Ori C. For this paper we added one more observation to the analysis for a net exposure of 83 ks. The availability of improved calibration products and models allowed us to refine these results in major areas. For Θ^1 Ori C the number of detected lines increased and allowed for better constraints on the plasma modeling specifically for the calculation of the DEM. The DEM analysis of the phase averaged spectrum as well as the fitting of the broad band plasma model showed that the bulk of the X-ray emission comes from plasmas with temperatures above 15 Million K and only a small, well separated part of the emission corresponds to emission of lower than 10 Million K.

There are models related to the standard line-driven wind instability model that are able to allow temperatures in excess of 10 Million K (Feldmeier et al. 1997a, Howk et al. 2000, Runacres&Owocki 2002). However possible high shock velocities near the onset of the wind cannot produce enough volume emissivity to account for the X-ray spectrum. The results also confirm a similar behavior for Θ^1 Ori A & E. This means the bulk of the X-ray emission in the bright Orion Trapezium stars is not compatible with any form of instabilities in a line-driven wind. In fact these stars seem to be of a hybrid nature where only a small fraction of the X-rays are produced in wind shocks, a larger fraction shows a magnetic origin and bears striking similarities to the hard X-ray emission pattern observed in stars with active coronae (Huenemoerder, Canizares, and Schulz 2001, Huenemoerder et al. 2003).

The DEM model allows for a non-thermal continuum component that contributes less than 1% to the total flux for a power law index of -0.5 as suggested by Chen and White (1991). These authors proposed a non-thermal origin for possible hard X-rays in form of an inverse Compton continuum. This limit corresponds to $4\times 10^{30}\text{ erg s}^{-1}$, which is an order of magnitude higher than predicted. Thus we may not really be sensitive to the issue. It is quite clear though that the high energy flux from the Orion Trapezium stars is not due to a possible non-thermal origin.

4.1. Possible Shocked Wind Component

The emissivity peak at $\log T = 6.9$ includes most lines from O to Si and ions below Fe XX. These are the moderate temperature lines we also observe in wind shocks in ζ Pup and others (Cassinelli et al. 2001, Kahn et al. 2001, Waldron and Cassinelli 2001, Schulz et al. 2001a, Schulz et al. 2002) suggesting a similar origin for this component on Θ^1 Ori C. This peak does not change within the two observed phases of the 15.4 day cycle in Θ^1 Ori C. Ignace (2001) and Owocki and Cohen (2001) calculated the shape of X-ray line profiles in stellar winds under various conditions.

The fact that most lines in the spectra do not show significant shifts and are unresolved puts limits on these conditions. If the lines were to be produced at large radii in the outer wind, we should observe broad, symmetric, sometimes flat topped lines. Yet for wind shocks, the only way to achieve symmetry is to have almost no attenuation in wind. Given the low mass loss rate of $\sim 4\times 10^{-7} M_{\odot}\text{ yr}^{-1}$ (Howarth & Prinja 1989) this is quite likely. Some of the X-ray emitting plasma also has to be near the photosphere at the onset of the wind given the unresolved nature of the lines. However it seems that some of the softest lines are indeed resolved and show velocity broadening of up to 850 km s^{-1} . This is indicative that these lines contributing to the

low temperature emissivity peak are due to X-rays from shocks in the outer wind. Would this low temperature emissivity be the only contribution to the X-ray emission, the Orion stars would be quite X-ray faint, but with a $\log L_x/L_{bol}$ between -7.2 and -7.6, which is near the canonical value for O stars.

4.2. Magnetically Confined Winds

The truth is, however, that $\log L_x/L_{bol}$ is more of the order of -6.5 for these stars. Since most emissivity appears to originate at temperatures that are incompatible with wind shocks, we have to look for other mechanisms. There are several indications that the enhanced X-ray activity could be triggered by magnetic fields. Gagne et al. (1997) interpreted the strong 15.4 day period in the X-ray and optical emission of Θ^1 Ori C reported by Stahl et al. (1996) in terms of the star's significant magnetic field.

Babel and Montmerle (1997a) proposed a magnetically confined wind shock (MCWS) model based on an oblique magnetic rotator model for Θ^1 Ori C. Here the wind is confined by a magnetic dipole field and forced into the magnetic equatorial plane. The observed 15.4 day variability thus is produced by the tilt of the dipole field relative to the rotational axis. The predicted field is of the order of 300 G. Very recent spectrophotometric observations indicate a dipole field of 1.1 kG with an inclination of 42° with respect to the stars rotational axis (Donati et al. 2002). These values are quite consistent with the temperatures we observe in the spectrum of Θ^1 Ori C. This model successfully explains the periodicity in the $H\alpha$ and H II lines as well as in P Cygni line profiles in the UV (Stahl et al. 1993, Walborn & Nichols 1994, Stahl et al. 1996, Reiners et al. 2000). In the X-ray light curve this interpretation of the periodicity is also attractive.

The HETG spectra, however, indicate a more complex behavior. The HETG observations were performed at phases around 0.37 and 0.82. According to the ROSAT HRI lightcurve in Gagne et al. (1997) we should see a difference in flux between the two observations of about 30%. This applies to the non-varying low temperature emissivity peak and we see the rise towards the first high temperature peak, which includes all the lines that were accessible to the ROSAT bandpass. The HETG data show that there is more going on than just a flux change. We observe a dramatic change of emissivity at $\log T$ (K) = 7.4 between the two phases. Donati et al. (2002) point out that meaningful comparisons with predictions of the MCWS model can only be achieved from lines at extreme configurations (phases 0.0 and 0.5). Our phase should be somewhere in between these two extremes. The model states that the change in luminosity between the two phases above 2 keV (below $\sim 6\text{\AA}$) should decrease compared to below 2 keV (above $\sim 6\text{\AA}$). This is not what we observe. The difference below 6\AA is largest instead with almost 40%. Furthermore we see no obvious reason in the MCWS, why the plasma temperature distribution should change like we observe in the DEM.

More quantitative modeling including a more detailed energy balance treatment by Ud'Doula and Owocki (2002) allow us to further differentiate the phenomenology between a magnetic field and a stellar wind. By relating the magnetic energy density to the matter outflow in the wind a confinement parameter $\eta \sim BR^2/\dot{M}v_\infty$ can be defined relating the magnetic field density at a radius R from the star and the mass loss rate \dot{M} in a stellar wind of terminal velocity v_∞ . Their magnetohydrodynamical simulations showed that in the case of a large η value

(~ 10) and closed magnetic field topologies near the star the wind is forced into loop-like structures in which strong shock collisions produce hard X-rays. Ud'Doula and Owocki (2002) showed that these structures could generate enough emissivity at high temperatures by applying the standard shock jump condition from Babel and Montmerle (1997b). For observed values of magnetic field strength, terminal wind velocity, and mass loss rates for Θ^1 Ori C, the η parameter is well over 10 (Gagne et al. 2001). Donati et al. (2002) applied the standard model devised by Babel and Montmerle (1997b) and found similar trends in terms of average temperature and density.

The loop-like structures proposed by Ud'Doula and Owocki (2002) and Gagne et al. (2001) may also explain the structure we observe in the DEM distribution where different peaks may relate to different confined structures. We can further speculate that changes at different phases refer to different structures. These confined structures may be quite unstable on short time scales resulting in highly variable X-ray emission. Feigelson et al. (2002) recently detect rapid variability in the O7pe star Θ^2 Ori A and suggested unseen companions for these stars (see also below). This may not be necessary. As an interesting analogy, the DEMs recently deduced from X-ray emission from active coronae in cool stars like AR Lac (Huenemoerder et al. 2003) and II Peg (Huenemoerder, Canizares, and Schulz 2001) appear very similar during flares, where in addition to a small low temperature peak one or more strong high temperature peaks evolve. The nature of the spectra in these cases are of striking similarity to the ones we observe in the Orion Trapezium with strong continua and unresolved lines. In this respect we may speculate that in the case of the Orion stars matter is constantly supplied into magnetic loops by the wind generating shock jumps on a permanent basis. In other words, these stars would be in a permanent state of flaring. The means of energy deposit is expected to be different in cool stars, which possess a dynamo and deposit energy into the plasma via reconnection. The mechanism in the winds of hot stars is more indirect via confining. Clearly, these details still have to be worked out.

If these shocks are magnetically confined they are not likely to produce line shifts and significant line broadening. Donati et al. (2002) simulated dynamic X-ray line spectra for several model cases for Θ^1 Ori C based on the MCWS model and found narrow line shapes at the observed phases. Any predicted line shifts are of the order of 150 to 200 km s⁻¹ and below our resolving power. This is consistent with the line characteristics in all three Orion spectra.

4.3. Low-Mass Companions

The Trapezium stars are known to have one or more companions. Quite recently Weigelt et al. (1999) reported on the existence of a close, probably low mass companion to Θ^1 Ori C and confirmed the companion detected by Petr et al. (1998) in Θ^1 Ori A. The companion in Θ^1 Ori C is as close as 33 milli-arcseconds. The close companion in Θ^1 Ori A has a separation of 202 milli-arcseconds. The only star in the Trapezium with no detected companion is Θ^1 Ori E. Based on the median age of the cluster of 0.3 Myr (Hillenbrandt 1997) and the ubiquity of nearby proplyds (O'Dell, Wen, & Hu 1993, Bally et al. 1998), which likely contain Class II T Tauri stars (Felli et al. 1993, McCaughrean & Stauffer 1994, Schulz et al. 2001), we consider these companions to be young T Tauri stars. Weigelt et al. (1999) similarly suggest that the companion in Θ^1 Ori C is a very young intermediate- or low-mass ($M < M_\odot$) star based

on evolutionary pre-main sequence (PMS) evolutionary tracks.

The X-ray emission of most young PMS stars in the Orion Trapezium Cluster is usually absorbed (Garmire et al. 2000), but emit hard X-ray emission with temperatures of around 30 Million K (Schulz et al. 2001). Giant X-ray flares can reach up to 60 to 100 Million K (Kamata et al. 1997, Yamauchi & Kamimura 1999, Tsuboi et al. 2000). X-ray contribution from such flares can be ruled out for Θ^1 Ori C, A, and E by the fact that we do not observe variability in the light curve (here we do not take in account high-frequency variability as observed by Feigelson et al. 2002). If we see contributions from the low-mass companion, it has to be persistent. X-ray luminosity functions from many star forming regions peak at luminosities below 10^{31} erg s $^{-1}$. This has also been observed for the low-mass PMS population in the vicinity of the Orion Trapezium (Schulz et al. 2001, Feigelson et al. 2002). In this respect a major contribution from such a companion to the spectrum in Θ^1 Ori C can be ruled out.

It is possible that X-rays from a low-mass companion make a significant contribution to Θ^1 Ori A, since its flux components are an order of magnitude fainter. Even if there were such a contribution, it can only be a small fraction of the total observed X-ray luminosity. This is even more the case for Θ^1 Ori E should it harbor an unseen companion. We can thus rule out that the X-ray emissivity pattern is due to a possible binary nature of the stars.

4.4. Evolutionary Implications

The very similar properties and morphologies in the spectra of Θ^1 Ori A, C, and E raises an intriguing issue. With an ionization age of the nebula of about 0.2 Myr and a median age of the cluster of about 0.3 Myr it is quite suggestive that the Trapezium stars are true ZAMS stars. Zero-age here is considered to be the time when energy generation by nuclear reactions first fully compensates the energy loss due to radiation from the stellar photosphere. In the case of Θ^1 Ori C it has been stated many times, that the magnetic activity could possibly be of pre-main sequence origin (Gagne et al. 2001, Donati et al. 2002). Gagne et al. (2002) noted that stars like Θ^1 Ori C, or τ Sco all show signs of magnetic activity and that they are all associated with young star-forming regions. With the Orion Trapezium we may have an indication that magnetic fields may be anti-correlated with age. Four out of the five main Trapezium stars now show strong magnetic signatures, with Θ^1 Ori A, C, and E the most striking cases. So far the view of primordial high fields has been limited to peculiar (Ap and Bp) stars and its has long been suspected that Θ^1 Ori C is a candidate for an Op star (Gagne et al. 2001). Θ^1 Ori D, so far also classified as a peculiar dwarf (B 0.5Vp), is weak in X-rays. The X-ray spectrum (Schulz et al. 2001) does not indicate very high temperatures and the grating data are too marginal to search for narrow lines. However, it seems that for some reason all Trapezium stars are chemically peculiar either by coincidence or this peculiarity has something to do with magnetism and/or their young age.

In Table 4 we list some properties from presumably young massive stars. These properties include the spectral type, the assumed cluster age, star forming region, and the currently known X-ray temperatures. The compilation is certainly far from complete, but demonstrates that stars from regions younger than 1 Million yr show clear evidence for magnetic activity. The main identifier for magnetic activity is the extremely high ($> 10^7$ K)

persistent temperature. For the Orion stars and τ Sco we additionally observe symmetric and narrow lines. HD 164492 is an interesting case as it is at the center of a very active star-forming region associated with the Trifid nebula, which very recently has been classified to be in a "pre-Orion" evolutionary stage (Lefloch & Cernicharo 2000) and thus maybe the "youngest" massive ZAMS star in the sample. Although not fully resolved, its X-ray characteristics (Rho et al. 2001) as observed with ASCA seem similar to what has been observed for Θ^1 Ori C with ASCA. Stars like HD 206267 and τ CMa are at the center of more evolved clusters and do not show these characteristics. In fact, they behave very much like ζ Pup (Kahn et al. 2001, Cassinelli et al. 2001) in that they show temperatures and line shapes consistent with shock instabilities in a radiation driven wind (Wojdowski et al. 2002, Schulz et al. 2001a, Schulz et al. 2002). Finally ι Ori and ζ Ori are part of the Orion region which is older than the Trapezium cluster core and further evolved. Here we also see no indication for magnetic activity (Schulz et al. 2002). ζ Ori (Waldron and Cassinelli 2001) maybe a special case in that it lacks high temperatures but possesses symmetric X-ray lines, which likely are due to a low opacity of the wind.

Table 4 may reflect an evolutionary sequence in which massive stars that enter the main sequence carry strong magnetic fields interacting with an emerging wind. In the table we list two types of X-ray luminosities based on the dichotomy observed in the Orion stars, L_x^{mag} for the amount produced by presumably magnetic confinement and L_x^{wind} for the amount from wind shocks. The bolometric luminosities for the L_x^{wind}/L_{bol} ratios were taken from Berghöfer, Schmitt, and Cassinelli (1996) Once the star evolves, magnetic fields may become less important as mass loss rates are higher. The X-ray emission sooner or later are fully generated by instabilities in the wind only. Here studies that search for magnetic fields in hot stellar winds (see Chesneau & Moffat 2002) are useful. An intriguing aspect on the Orion stars is that there also seems to exist relatively faint X-ray emission consistent with non-magnetic wind shocks. Thus even if it is the case that most Orion stars are indeed just abnormal and strong magnetic fields are more the exception than the rule, then very young massive stars if not magnetic should at least scale with their bolometric luminosity with $L_x^{wind}/L_{bol} \sim -7$ and not higher. This may explain the relative X-ray weakness of HD 164492 A relative to Θ^1 Ori C (J. Rho, private communication), although Θ^1 Ori C may be even younger than HD 164492 A. This may not explain the extremely weak X-rays flux from Θ^1 Ori D, though. From a projected bolometric luminosity for a B0.5V star of 10^{38} erg s $^{-1}$ and an X-ray luminosity of 3×10^{29} erg s $^{-1}$ (from Schulz et al. 2001) we compute a L_x^{wind}/L_{bol} of -8.5 for the star, which is very low. On the other hand we can turn the argument around and in the case of τ Sco use $L_x^{wind}/L_{bol} = -7$ to estimate the amount of L_x^{mag} out of the observed ratio as has been in done in Table 3.

Too little is known about massive stars as they quickly evolve towards the main sequence. Although it is well accepted that many high-energy processes in YSOs are dominated by magnetic activity (see Feigelson & Montmerle 1999 for a review) and hard X-rays in flares are produced by powerful magnetic reconnections, star-disc activities and jet-formation, these findings are still confined to low mass stars. In several models for class I and II YSOs magnetic field play a crucial role in the X-ray production, either in form of X-ray winds and accretion (Shu et al. 1997) or accretion shocks (Hartmann 1998). It has yet to be established how these models for low-mass YSOs may

TABLE 4 YOUNG MASSIVE STARS VS. MAGNETIC ACTIVITY

star	spectral type	age My	Star Form. Region	T MK	Magn. Fields	$\log L_x^{mag}$ erg s ⁻¹	$\log L_x^{wind}$ erg s ⁻¹	$\log L_x^{wind}/L_{bol}$	refs. ^a
Θ^1 Ori A	B0.5V	0.3	Orion	5-43	yes	31.0	30.7	-7.3	1,2,3
Θ^1 Ori B	B1V/B3	0.3	Orion	22-35	prob.	30.3	?	?	2,3,4
Θ^1 Ori C	O6.5Vp	0.3	Orion	6-66	yes	32.2	31.5	-7.2	1,2,3
Θ^1 Ori D	B0.5Vp	0.3	Orion	7-8	?	?	29.5	-8.5	2,3,4
Θ^1 Ori E	B0.5	0.3	Orion	4-47	yes	31.4	30.8	-7.2	1,2,3
Θ^2 Ori	O9.5Vpe	0.3	Orion	5-32	yes	31.1	31.4	-7.1	7,12
τ Sco	B0.2V	~1	Sco-Cen	7-27	yes	31.9	31.4	-7	5,6
HD 164492A	O7.5V	0.3	Trifid	2-12?	?	?	31.4	7.1	8,8a
HD 206267	O6.5V	3-7	IC 1396	2-10	no	-	31.6	-7.7	9,10
τ CMA	O9 Ib	3-5	NGC 2362	3-12	no	-	32.3	-7.2	9
15 Mon	O7V	3-7	NGC 2264	2-10	no	-	31.7	-7.2	
ι Ori	O9 III	<12	Orion	1-10	no	-	32.4	-6.8	9
ζ Ori	O9.7 Ib	<12	Orion		no	-	32.5	-6.8	11
δ Ori	O9.5II	<12	Orion		no	-	32.2	-6.8	13

^a (1) this paper; (2) Hillenbrandt (1997); (3) Petr et al. (1998); (4) Schulz et al. (2001); (5) Cohen, Cassinelli & Waldron (1997); (6) Killian (1994); (7) Schulz et al. (2003a); (8) Rho et al. (2001); (8a) J. Rho, priv. comm.; (9) Wojdowski et al. (2002); (10) Strickland et al. (1997); (11) Waldron & Cassinelli (2001); (12) Feigelson et al. (2002); (13) Miller et al. (2002)

relate to more massive stars.

One should be careful, however, to simply argue with age in such a correlation. It has to be kept in mind that there are similar patterns once we include mass loss rate and wind velocities. In this respect the stars associated with magnetic activity also have low mass loss rates, low wind velocities and many of them are optically classified as dwarfs. All these properties have to be accounted for. Future studies need to incorporate a large number of highly resolved X-ray spectra of these young massive stars in correlation with fundamental stellar wind prop-

erties to establish an evolutionary pattern that leads from either faint or magnetically dominated X-ray sources to strong wind instability dominated X-ray sources.

We thank all the members of the *Chandra* team for their enormous efforts and the referee for valid comments to improve the manuscript. This research is funded in part by the Smithsonian Astrophysical Observatory contract SV-61010 (CXC) and NAS8-39073 (HETG) under the Marshall Space Flight Center.

REFERENCES

- Babel J., & Montmerle T., 1997b, A&A 323, 121
 Babel J., & Montmerle T., 1997a, ApJ 485, L29
 Bally J., Sutherland R.S., Devine D., and Johnstone D., 1998, AJ 116, 293
 Berghöfer T.W., and Schmitt J.H.M.M., 1994, A&A 292, L5
 Berghöfer T.W., Schmitt J.H.M.M., and Cassinelli J.P., 1996, A&A 31, 289
 Blumenthal G.R., Darke G.W.F., and Tucker W.H., 1972, ApJ 172, 205
 Bohlin R.C. & Savage B.D., 1981, ApJ 249, 109
 Birkhouse N.S., Dupree A.K., Edgar R.J., Liedahl D.A., Crake S.A., White N.E., and Singh K.P., 2000, ApJ 530, 387
 Casinelli J.P., Miller N.A., Waldron W.L., MacFarlane J.J., and Cohen D.H., 2001, ApJ 554, 55
 Casinelli J.P., Cohen D.H., MacFarlane J.J., Sanders W.T., and Welsh B.Y., 1994, ApJ 421, 705
 Cassinelli J.P. and Swank J.H., 1983, ApJ 271, 681
 Chavez M., Stalio R., and Holberg J.B., 1995, ApJ 449, 280
 Chen W., & White R.L., 1991, ApJ 366, 512
 Chesneau O. & Moffat A.F.J., 2002, PASP 114, 612
 Chlebowski T., Harnden F.R. jr., and Sciortino S., 1989, ApJ 341, 427
 Cohen D.H., de Messières G.E., MacFarlane J.J., Miller, N.A., Cassinelli J.P., Owocki, S.P., and Liedahl, D.A., 2002, ApJ, submitted
 Cohen D.H., Cassinelli J.P., and Waldron W.L., 1997, ApJ 488, 397
 Cohen D.H., Cassinelli J.P., and MacFarlane J.J., 1997, ApJ 487, 867
 Cohen D.H., Cooper R.G., MacFarlane J.J., Owocki S.P., Cassinelli J.P., and Wang P., ApJ 460, 506
 Corcoran M.F., Waldron W.L., MacFarlane J.J., et al., 1994, ApJ 436, L95
 Donati J.-F., Babel J., Harries T.J., Howarth I.D., Petit P., and Semel M., 2002, MNRAS 333, 55
 Drake G.W., 1971, Phys. Rev. A, 3, 908
 Feigelson E.D., Broos P., Gaffney J.A. III, Garmire G., Hillenbrand L.A., Pravdo S.H., Townsley L., and Tsuboi Y., 2002, ApJ 574, 258
 Feigelson E.D., and Montmerle T., 1999, ARA&A 37, 363
 Feldmeier A., Kudritzki R.P., Palsa R., Pauldrach A.W., and Puls J., 1997, A&A 320, 899
 Feldmeier A., Puls J., and Pauldrach A.W., 1997, A&A 322, 878
 Felli M., Taylor G.B., Catarzi M., Churchwell E., and Kurtz S., 1993, A&ASuppl. 101, 127
 Gagne, M., Cohen, D., Owocki, S., and Ud-Doula, A., 2001, in X-ray at Sharp Focus, ASP Conference Series, eds. S. Vrtilik, E.M.Schlegel, L. Kuhl
 Gagné M., Caillault J.-P., and Stauffer J.R., 1995, ApJ 445, 280
 Gagné M., Caillault J.-P., Stauffer J.R., and Linsky J.L., 1997, ApJ 478, L87
 Garmire G., Feigelson E.D., Broos P., Hillenbrand L., Pravdo S.H., Townsley L., and Tsuboi Y., 2000, AJ 120, 1426
 Huenemoerder D.P., Canizares C.R., Drake J.J., and Sanz-Forcada J., 2003, ApJ, submitted
 Huenemoerder D.P., Canizares C.R., and Schulz N.S., 2001, ApJ 559, 1135
 Harnden F.R. jr., Branduardi G., Gorenstein P., Grindlay J., Rosner R., Topka K., Elvis M., Pye J.P., and Vaiana G.S., 1979, ApJ 234, 55
 Hillier D.J., Kudritzki R.P., Pauldrach A.W., Baade D., Casinelli J.P., Puls J., and Schmitt J.H.M.M., 1993, A&A 276, 117
 Hillenbrand L.A., 1997, AJ 113, 1733
 Howarth I.D. & Prinja R.K., 1989, ApJS 69, 527
 Howk J.C., Cassinelli J.P., Bjorkman J. E., Lamers H.J.G.L.M., 2000, ApJ 534, 348
 Huenemoerder D., Canizares C.R., and Schulz N.S., 2001, ApJ 559, 1135
 Ignace R., 2001, ApJ 549, 119
 Kahn, S.M., Leutenegger, M., Cottam, J., Rauw, G., Vreux, J.M., den Boggende, T., Mewe, R., & Guedel, M., 2001, A&A, 365, L312

- Kamata Y., Koyama K., Tsuboi Y., and Yamauchi S., 1997, PASJ 69, 461
 Kilian J., 1994, A&A 282, 867
 Lamers H.J.G.L.M. and Cassinelli J.P., 1999, Introduction to Stellar Winds, Cambridge Univ. Press, Cambridge
 Lefloch B & Cernicharo J., ApJ 545, 340
 Lucy L.B., and White R.L., 1980, ApJ 241, 300
 Lucy L.B., 1982, ApJ 255, 286
 MacFarlane J.J., Waldron W.L., Corcoran M.F., Wolff M.J., Wang P., and Casinelli J.P., 1993, ApJ 419, 813
 Mazzotta P., Mazzitelli G., Colafrancesco S., and Vittorio N., 1998, A&ASuppl. 133, 403
 McCaughrean M.J., and Stauffer J.R., 1994, AJ 108, 1382
 Mewe R., and Schrijver J., 1978, A&A 65, 99
 Miller N.A., Casinelli J.P., Waldron W.L., MacFarlane J.J., and Cohen D.H., 2002, ApJ 577, 951
 Nordsieck K.H., Cassinelli J.P. and Anderson C.M., 1981, A&A 248, 678
 O'dell C.R., Wen Z., and Hu X., 1993, ApJ 410, 696
 Owocki S.P., Castor J.I., and Rybicki G.B., 1988, ApJ 335, 914
 Owocki S.P., & Cohen D.H., 2001, ApJ 559, 1108
 Pallavicini R., Golub L., Rosner R., Vaiana G.S., Ayres T., and Linsky J.L., 1981, ApJ 248, 279
 Pauldrach A.W., Kudritzki R.P., Puls J., Butler K., and Hunsinger J., 1994, A&A 283, 525
 Petr M.G., Coudé du Foresto V., Beckwith S.V.W., Richichi A., and McCaughrean M.J., 1986, ApJ 500, 825
 Predehl P. & Schmitt J.H.M.M., 1995, A&A 293, 889
 Puls J., Owocki S.P., and Fullerton A.W., 1993, A&A 279, 457
 Rho J., Corcoran M.F., Chu, Y.-H., and Reach, W.T., 2001, ApJ 562, 446
 Reiners A., Stahl O., Wolf B., Kaufer A., and Rivinius T., 2000, A&A 363, 585
 Runacres M.C. & Owocki S.P., 2002, A&A 381, 1015
 Savage B.D. & Jenkins E.P., 1972, ApJ 172, 491
 Schulz N.S., Canizares C.R., Huenemoerder D., and Lee J., 2000, ApJ 545, L135
 Schulz N.S., Canizares C.R., Huenemoerder D., Kastner J.H., Taylor S.C., and Bergstrom E.J., 2001, ApJ 549, 441
 Schulz N.S., Huenemoerder D., Kastner J.H., and Lee J., 2001a, AAS 198, 2205
 Schulz N.S., 2002, in "Winds, Bubbles, and Explosions, eds. J. Arthur and R. Dyson, Patzcuaro
 Schulz N.S., Canizares C.R., Huenemoerder D., Kastner J.H., Taylor S.C., and Bergstrom E.J., 2003, ApJ, erratum submitted
 Seward F.D., Froman W.R., Giacconi R., Griffith R.E., Harnden F.R. jr., Jones C., Pye J.P., 1979, ApJ 234, 55
 Smith R.K., Brickhouse N.S., Liedahl D.A., and Raymond J.C., 2001, ApJ, 556, 91
 Snow T.P. & Jenkins E.B., 1977, ApJS 33, 269
 Spitzer, L. 1978, Physical Processes in the Interstellar Medium (New York: Wiley)
 Stahl O., Wolf B., Gäng T., Gummersbach C., Kaufer A., Kovács J., Mandel H., Szeifert T., 1993, A&A 274, L29
 Stahl O., Kaufer A., Rivinius T., Seifert T., Wolf B., Gäng T., Gummersbach C.A., Jankovics I., Kovacs J., Mandel H., Pakull M.W., and Peitz J., 1996, A&A 312, 539
 Tsuboi Y., Imanishi K., Koyama K., Grosso N., and Montmerle T., 2000, ApJ 532, 1089
 Ud-Doula A. & Owocki S.P., 2002, ApJ 576, 413
 Walborn N. & Nichols J.S., 1994, ApJ 425, L29
 Waldron, W.L., & Cassinelli, J.P., 2001, ApJ, 548, L45
 Waljeski K., Moses D., Dere K., Saba J.L.R., Strong K.T., Webb D.F., and Zarro D.M., 1994, ApJ 429, 909
 Weigelt G., Balega Y., Preibisch T., Schertl D., Schöller M., and Zinnecker H., 1999, A&A 347, L15
 Wojdowski P.S., Schulz N.S., Ishibashi K., & Huenemoerder D., in *High Resolution X-ray Spectroscopy with XMM-Newton and Chandra*, MSSL, Oct. 2002
 Yamauchi S., & Koyama K., 1993, ApJ 404, 620
 Yamauchi S., Koyama K., Sakano M., and Okada K., 1996, PASJ 48, 719
 Yamauchi S., and Kamimura R., 1999, "Star Formation 1999", sf99.proc, 308Y